Plasmonics (2011) 6:659–664
DOI 10.1007/s11468-011-9248-x

Optical Transmission Enhancement and Tuning by Overlaying Liquid Crystals on a Gold Film with Patterned Nanoholes

Y. J. Liu · Eunice S. P. Leong · B. Wang · J. H. Teng

Received: 4 March 2011 / Accepted: 5 July 2011 / Published online: 12 July 2011

Abstract A gold film with subwavelength nanoholes on a glass substrate was fabricated through electron beam lithography and its extraordinary optical transmission (EOT) was characterized. By applying a liquid crystal overlayer to the gold film, its EOT can be further enhanced by ~11% due to the refractive index matching of the dielectric media on its two sides. By controlling the alignment of the liquid crystal molecules, a highly reversible and reproducible tuning of the transmission peak in both intensity and position is demonstrated.

Keywords Optical transmission · Nanohole array · Dual-frequency liquid crystal · Surface plasmon polariton

Introduction

The discovery of extraordinary optical transmission (EOT) through a metal film perforated with two-dimensional nanohole arrays has attracted intense attention since it was first reported in 1998 [1]. Different physical models have been proposed to explain the unusual transmission enhancement, such as surface plasmon polariton (SPP) models [1–3], composite diffracted evanescent wave models [4, 5], dynamical diffraction [6], waveguide mode [7], and cavity resonances [8]. Though the mechanism for the transmission enhancement is still under debate, researchers have found that the EOT in visible, near infrared, and terahertz range is sensitive to many physical and geometrical parameters including the film material [9–11], film thickness [12–14], geometry symmetry [15–19], lattice constant [16, 20–23], as well as hole size [20, 24–27] and hole shape [28–32]. This provides us with many degrees of freedom for the manipulation of light propagation. EOT has great potential for many applications such as organic light-emitting diodes [33], nanolithography [34], color filters [35], and sensors [36].

The evanescent nature of the SPPs makes them extremely sensitive to dielectric properties of the surrounding material in the vicinity of the metal surface. As a result, changing the dielectric properties of a material in contact with the metallic nanohole array will lead to a change in the transmission spectrum. Various approaches have been explored to control the SPP dispersion and subsequent optical transmission based on different materials, such as liquid crystals (LCs) [37–39] and J-aggregates [40]. However, J-aggregates-based systems tend to be unstable after repeated switching due to the photo-induced decay. In contrast, LC-based systems are much more stable with acceptable response and high fidelity but only based on nematic LCs with positive dielectric anisotropy. To further strengthen their potential in plasmonic applications, it is therefore highly desirable to explore other types of LCs, for instance, dual-frequency LCs.

In this letter, we demonstrate a hybrid system with enhanced EOT by applying a nematic dual-frequency liquid crystal (DFLC) to a uniform Au nanohole array. Such a DFLC can change the sign of dielectric anisotropy between positive and negative when the frequency of the applied electric field changes [41–44], thus changing the EOT of the hybrid system. By overlaying the DFLC onto the Au nanohole array, we achieved ~11% enhancement in transmittance compared to the bare Au nanohole array. In

Y. J. Liu (✉) · E. S. P. Leong · B. Wang · J. H. Teng (✉)
Institute of Materials Research and Engineering,
Agency for Science Technology and Research (A*STAR),
3 Research Link,
Singapore 117602, Republic of Singapore
e-mail: liuy@imre.a-star.edu.sg
e-mail: jh-teng@imre.a-star.edu.sg

addition, the EOT can be frequency tuned by electrically controlling the alignment of the DFLC molecules.

Simulation and Experiments

Figure 1a shows the schematic diagram of a gold nanohole array patterned on an indium-tin-oxide (ITO) glass substrate. The structural parameters related to the device are denoted as: Λ for the pitch of the grating, L and W for the length and width of each rectangular hole, G_1 and G_2 for the width of metal stripes in between two adjacent aperture holes along x- and y-directions, and H for the grating height. Here, Λ is shorter than the optical wavelength (450−750 nm).

The proposed device was theoretically analyzed using the rigorous coupled wave analysis method [45]. The dispersion information associated with the Au was derived from the fitting of tabulated data [46]. The glass substrate was assumed to possess a constant refractive index of 1.52 with negligible optical loss in the interested wavelength range. The wavelength-dependent refractive index of ITO was deduced from the fitting of experimental data [47]. The nanohole height was set to be the same as the thickness of the metal layer throughout this work.

In our experiments, the highly ordered gold nanohole array on an ITO glass substrate was fabricated based on the standard e-beam lithography. In brief, a 250-nm-thick e-beam resist (PMMA 950k) was spin coated on the pre-treated ITO glass substrate, followed by 15 min baking at 170 °C. After e-beam exposure, the patterns were then developed in n-amyl acetate at 20 °C for 3 min, followed by immersing into methyl isobutyl ketone: isopropanol (IPA)=1:3 solvent for 70 s and rinsing in IPA for 30 s. After O_2 plasma descum, a chromium adhesion layer (5 nm) and a gold layer (50 nm) were subsequently deposited in vacuum over the pattern. Finally, a well-patterned gold nanohole array on the ITO glass substrate was produced by removing the resist in Acetone solution.

A field emission scanning electron microscope (SEM) image of the fabricated nanohole array is shown in Fig. 1b, from which the aforementioned parameters are determined: Λ=320 nm, L=180 nm, W=160 nm, G_1=140 nm, G_2=160 nm. The whole working area of the Au nanohole array is 3.5×3.5 mm^2.

A monolayer of hexadecyl trimethyl ammonium bromide [48] was self-assembled on both the bare ITO glass substrate and the substrate with Au nanohole array. These two substrates, serving as electrodes, were assembled together to form a LC cell. The cell thickness was controlled to be ~2 μm using the polystyrene microbeads. After injection of LCs, the homeotropic alignment of LCs was achieved: LC molecules align perpendicular to the substrates. The DFLC material used was MLC-2048 (Merck), which has the positive sign of dielectric anisotropy, $\Delta\varepsilon = \varepsilon_{//} - \varepsilon_{\perp} > 0$, when the frequency f of the applied electric field smaller than the crossover frequency f_c= 12 kHz (at 20 °C) and a negative sign, $\Delta\varepsilon<0$, when $f>f_c$ [49]. Here, $\varepsilon_{//}$ and $\varepsilon_{\perp}$ are the dielectric permittivities of the DFLCs in the directions parallel and perpendicular to the LC director, respectively. For LCs with $\Delta\varepsilon>0$, the director prefers to align toward the electric field direction; while for $\Delta\varepsilon<0$, it realigns perpendicularly to the field. Figure 1c and d shows the schematic drawings of the alignment of DFLC molecules when they are completely switched at the

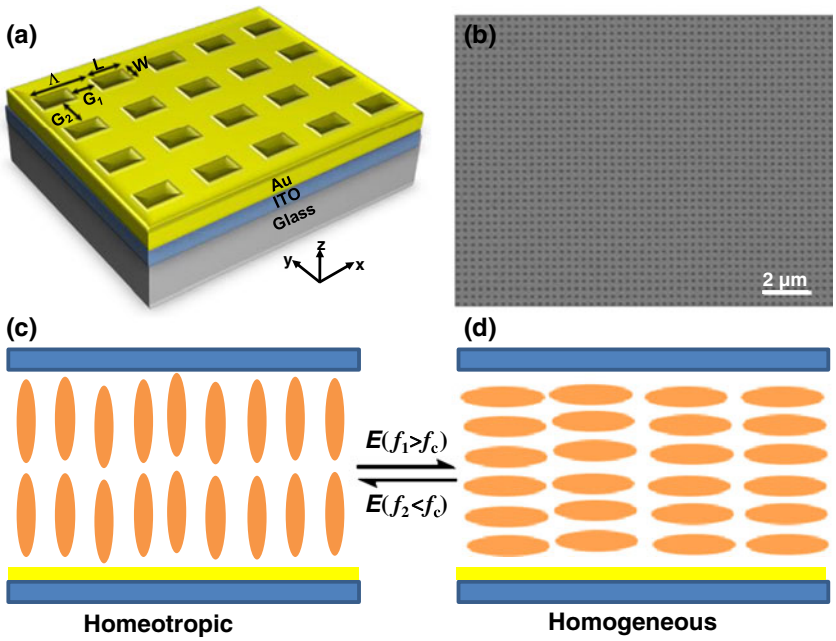

Fig. 1 Schematic of subwavelength patterned gold nanohole structures (**a**), SEM image of an Au nanohole array on an ITO glass substrate (**b**), and reversible switching between the homeotropic (**c**) and homogeneous (**d**) alignment of DFLC molecules. (Color online)

frequency below and above the crossover frequency, respectively. For the DFLCs used in this experiment, it has an ordinary refractive index n_o=1.4978 and an extraordinary refractive index n_e=1.7192, giving an optical birefringence of Δn=0.2214 (all at λ=589 nm).

Optical transmission spectra were measured with an unpolarized probe light beam using a UV-Vis-NIR microspectrophotometer (CRAIC QDI 2010™). The probe light beam was focused to have a detecting area of 31×31 μm^2 using an objective lens. It is worth mentioning that due to the limitation of the spectrophotometer, the spectrum can be only measured for unpolarized probe light in our experiments.

Results and Discussion

Figure 2a and b shows the calculated and tested transmittance spectra for a continuous Au film and Au nanohole structure with and without DFLC overlayer for normally incident unpolarized light. From Fig. 2, it is obvious that there exists a transmission peak at ~500 nm for the continuous Au film, which results from the electrons transition and recombination between the filled *d*-bands and the Fermi level in conduction band [50–52]. It is noted that this peak is present in all of our spectra, independent of structure properties and overlaying materials. This observation indicates that the light coupling with surface plasmons induced by the periodic nanoholes is not a dominant factor for the transmission characteristics at ~500 nm. In contrast, a pronounced transmission peak at ~690 nm appears in the perforated Au nanohole film in addition to the same transmission peak at ~500 nm as the continuous Au film. This transmission peak is a result of light coupling with the surface plasmons along the nanohole array structure. Interestingly, a trough with the dip position at ~590 nm also appears between two transmission peaks, which can be attributed to the localized surface plasmon resonance. When a DFLC overlayer is applied on the perforated one, we can observe from both simulation and experimental results that the *d*-bands transmission peak at ~500 nm does not shift while both the peak and trough induced by surface plasmons have red shifts. It is well known that periodic arrays can provide the additional momentum required to couple incoming light to SPPs; in a square array of nanoholes the peak positions can be approximately estimated as $\lambda_{max} = \left(\Lambda/\sqrt{n_x^2 + n_y^2}\right)\sqrt{\varepsilon_d \varepsilon_m/(\varepsilon_d + \varepsilon_m)}$ [22], where ε_d and ε_m are the dielectric function of the dielectric and the metal, respectively, Λ is the lattice constant of the array, and n_x and n_y are integers. From the equation, only ε_d changes from ε_{air} to ε_{LC} in our experiment when the DFLC overlayer is applied on the gold nanohole array. By substituting the dielectric constants of the dielectric and metal into this equation, the resulting λ_{max} gets red-shifted. Therefore, we can see from Fig. 2 that the transmission peak has a shift of ~104 nm (from ~724 to ~828 nm) in the theoretical calculation and a shift of ~120 nm (from ~690 to ~810 nm) in the measured spectrum, while the trough has a theoretical shift of ~47 nm (from ~610 to ~657 nm) and an experimental shift of ~70 nm (from ~590 to ~660 nm). More importantly, the transmittance of both peaks increases greatly by applying the DFLC overlayer but the peak at ~810 nm has much higher transmission than the one at ~500 nm. The theoretical and experimental peak transmittance is enhanced by ~9% and ~11% compared to the bare case. We believe that the application of the DFLC overlayer to the perforated metal layer leads to an index matching of the media on both sides of it, thus further boosting the optical transmission. From Fig. 2a–b, we also note that the peak to trough depth from the theoretical calculation is much larger than that from the experimental results. This difference was attributed to the

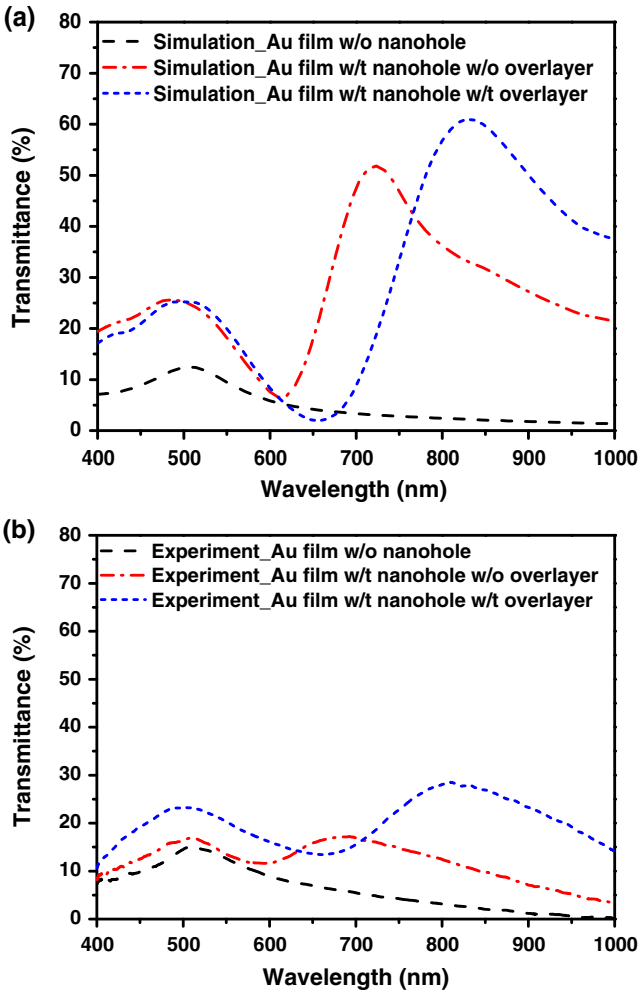

Fig. 2 Simulated (**a**) and experimental (**b**) results of the transmittance for a continuous Au film and Au nanohole structures with and without DFLC overlayer (homeotropic alignment) for normally incident unploarized light. (Color online)

scattering caused by the LC layer. Under a polarized optical scope, we observed that there existed many defect-induced LC domains inside the LC layer, which caused relatively strong scattering and hence decreased the transmittance of this hybrid system. It is worth noting that the nanoholes are assumed to be rectangular in theoretical calculation, while their four corners are not really sharp from the SEM image, thus resulting in slight difference between the theoretical calculation and experimental data.

Figure 3a and b show the voltage-dependent transmittance spectra when the frequency was fixed at 1 and 22 kHz, respectively. When a low-frequency (f=1 kHz) electric field is applied to the cell, the LC molecules with $\Delta\varepsilon>0$ are aligned more orderly (perpendicular to the substrates). In this case, regardless of the polarization of the probe light, it will only see the ordinary refractive index, n_o, of the DFLCs. However, we believe that the LC molecules in the nanoholes are independent of external electric field due to the strong anchoring energy of the nanoholes and also demonstrate an isotropic state: $n_{iso} \cong (2n_o + n_e)/3 = 1.5716$ [53]. There is therefore a slight decrease in transmittance caused mainly by more ordered alignment of the positive anisotropic molecules by the applied field (Fig. 3a). When a high-frequency (f=22 kHz) voltage is applied, the DFLC exhibits a negative dielectric anisotropy ($\Delta\varepsilon<0$). As the applied voltage increases, the LC molecules are switched into horizontal alignment, as illustrated in Fig. 3b. Although the LC domains are perpendicular to the electric field, they may rotate within the plane. Statistically, an unpolarized incoming beam will see an average of the ordinary and extraordinary indices. Therefore, the effective refractive index at a high frequency can be written as $n_{hf} \cong \sqrt{(n_o^2 + n_e^2)/2} = 1.6123$, which is larger than that of the homeotropic alignment. Consequently, the transmission peak and trough are slightly red-shifted. In addition, there is a dramatic decrease in the peak transmittance (from ~28% to ~15%). In our experiments, we observed that there were many LC domains formed under the applied electric field with high frequency, which caused strong scattering of the incoming light. As a result, the transmittance of the hybrid system in the whole spectral range has an obvious decrease.

For LC-based systems, a distinct advantage is that their optical properties can be dynamically controlled. In our experiments, reversible tuning of the transmission was achieved by manually switching the electric field on and off at the fixed frequency of 22 kHz using an He–Ne laser (633 nm). The dynamic transmission change was captured by an oscilloscope. Figure 4 shows the response time of this DFLC-based hybrid system at the applied voltage of 16 V. The measured rising time and falling time are ~60 ms and ~270 ms, respectively. Huang et al. [54] have reported that the rising time τ_{on} and falling time τ_{off} of the DFLC-

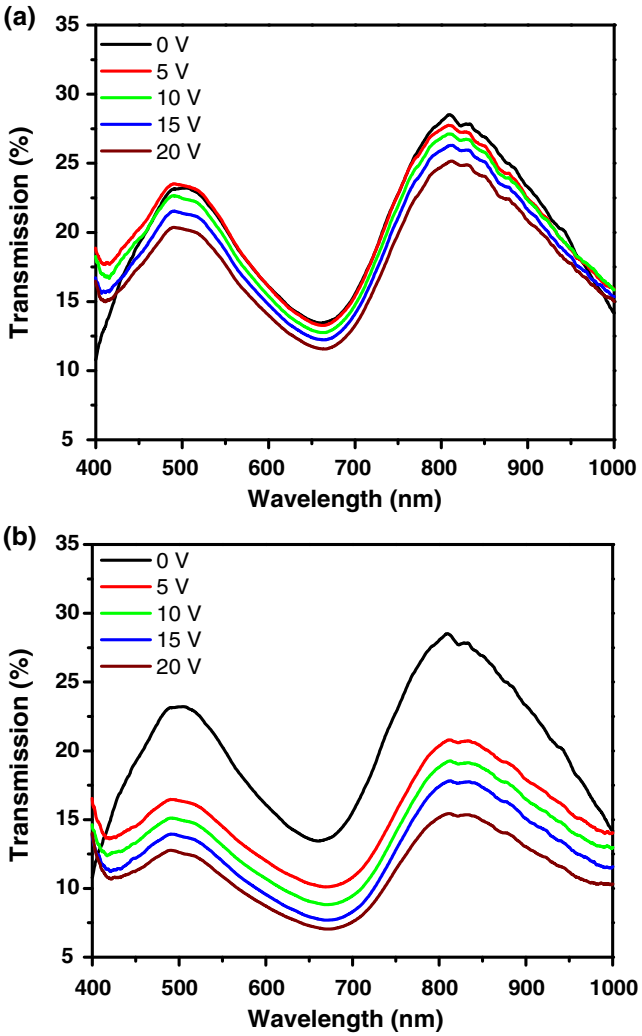

Fig. 3 Voltage-dependent transmittance spectra with the frequency fixed at 1 kHz (**a**) and 22 kHz (**b**), respectively. (Color online)

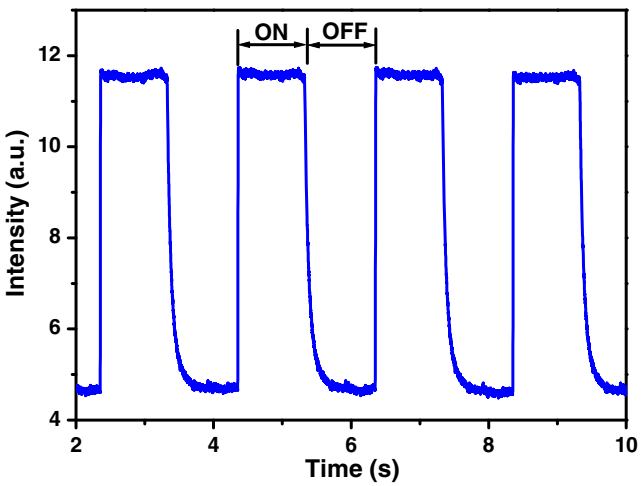

Fig. 4 Dynamic response under the applied voltage of 16 V with the frequency of 22 kHz. (Color online)

based device driven by relatively high voltages can be written as $\tau_{on} = \gamma_1 d^2/(\varepsilon_0|\Delta\varepsilon|V^2 - k_{eff}\pi^2) \cong \gamma_1/(\varepsilon_0|\Delta\varepsilon|E^2)$ and $\tau_{off} = \gamma_1 d^2/(k_{eff}\pi^2)$, where d is the cell thickness, γ_1 is the viscosity, k_{eff} is the effective elastic constant, and E is the applied electric field. We can see that the rising time is inversely proportional to E^2 while the falling time is a self-relaxation process, depending on the material intrinsic properties. Faster response time can be achieved by using specially designed driving electrodes [55]. The observed dynamic response of the transmission under the applied electric field indicates that the hybrid system is highly reversible and reproducible.

Conclusion

We have fabricated a gold film with subwavelength nanohole arrays on an ITO glass substrate and observed EOT at ~690 nm. By overlaying a DFLC layer to the gold nanohole array, the EOT can be further enhanced by ~11% due to index matching. Since the alignment of the DFLC molecules can be efficiently controlled by the frequency of applied electric field, the tuning behavior of the transmission peak in both intensity and position is highly reversible and reproducible. Our future work will be further improving the performance by optimizing its structural parameters, such as the metal thickness and the duty ratio, and investigating different nanohole shapes on the EOT, such as circles and triangles. This DFLC-based subwavelength patterned metallic structures can be potentially used in many applications such as switches, lenses, and color filters.

Acknowledgment This work was financially supported by Agency for Science, Technology and Research (A*STAR), under the grant No. 0921540099 and 0921540098.

References

1. Ebbesen TW, Lezec HJ, Ghaemi HF, Thio T, Wolff PA (1998) Nature 391:667–669
2. Martin-Moreno L, Garcia-Vidal FJ, Lezec HJ, Pellerin KM, Thio T, Pendry JB, Ebbesen TW (2001) Phys Rev Lett 86:1114–1117
3. Liu HT, Lalanne P (2008) Nature 452:728–731
4. Lezec HJ, Thio T (2004) Opt Express 12:3629–3651
5. Gay G, Alloschery O, Lesegno BVD, O'dwyer C, Weiner J, Lezec HJ (2006) Nat Phys 2:262–267
6. Treacy MMJ (2002) Phys Rev B 66:195105
7. Bravo-Abad J, Martin-Moreno L, Garcia-Vidal FJ (2004) Phys Rev E 69:026601
8. Popov E, Neviere M, Enoch S, Reinisch R (2000) Phys Rev B 62:16100–16108
9. Azad AK, Zhao YG, Zhang WL, He MX (2006) Opt Lett 31:2637–2639
10. Garcia N, Nieto-Vesperinas M (2007) J Opt A Pure Appl Opt 9:490–495
11. Chang YT, Chuang TH, Yang C-H, Tsai MW, Lee SC (2007) Appl Phys Lett 90:213101
12. Fang X, Li ZY, Long YB, Wei HX, Liu RJ, Ma JY, Kamran M, Zhao HY, Han XF, Zhao BR, Qiu XG (2007) Phys Rev Lett 99:066805
13. Vallius T, Turunen J, Mansuripur M, Honkanen S (2004) J Opt Soc Am A 21:456–463
14. Degiron A, Lezec HJ, Barnes WL, Ebbesen TW (2002) Appl Phys Lett 81:4327–4329
15. Sun M, Tian J, Han S, Li ZY, Cheng BY, Zhang DZ, Jin A, Yang HF (2006) J Appl Phys 100:024320
16. Wang QJ, Li JQ, Huang CP, Zhang C, Zhu YY (2005) Appl Phys Lett 87:091105
17. Li JQ, Yang WQ, Zhang YT, Wang QJ, Huang CP, Zhu YY (2007) J Appl Phys 101:073505
18. Przybilla F, Genet C, Ebbesen TW (2006) Appl Phys Lett 89:121115
19. Papasimakis N, Fedotov VA, Schwanecke AS, Zheludev NI, de Abajo FJ Garcia (2007) Appl Phys Lett 91:081503
20. Biswas R, Neginhal S, Ding CG, Puscasu I, Johnson E (2007) J Opt Soc Am B 24:2589–2596
21. Salomon L, Grillot F, Zayats AV, de Fornel F (2001) Phys Rev Lett 86:1110–1113
22. Ghaemi HF, Thio T, Grupp DE, Ebbesen TW, Lezec HJ (1998) Phys Rev B 58:6779–6782
23. Fan W, Zhang S, Minhas B, Malloy KJ, Brueck SRJ (2005) Phys Rev Lett 94:033902
24. Li JY, Li ZY, Yang HF, Jin AZ (2008) J Appl Phys 104:114303
25. van der Molen KL, Segerink FB, van Hulst NF, Kuipers L (2004) Appl Phys Lett 85:4316–4318
26. Thio T, Ghaemi HF, Lezec HJ, Wolff PA, Ebbesen TW (1999) J Opt Soc Am B 16:1743–1748
27. Ruan ZC, Qiu M (2006) Phys Rev Lett 96:233901
28. Clark AW, Sheridan AK, Glidle A, Cumming DRS, Cooper JM (2007) Appl Phys Lett 91:093109
29. Strelniker YM (2007) Phys Rev B 76:085409
30. Masson JB, Gallot G (2006) Phys Rev B 73:121401(R)
31. Klein Koerkamp KJ, Enoch S, Segerink FB, van Hulst NF, Kuipers L (2004) Phys Rev Lett 92:183901
32. Degiron A, Ebbesen TW (2005) J Opt A Pure Appl Opt 7:S90–S96
33. Gifford DK, Hall DG (2002) Appl Phys Lett 81:4315–4317
34. Srituravanich W, Fang N, Sun C, Luo Q, Zhang X (2004) Nano Lett 4:1085–1088
35. Lee HS, Yoon YT, Lee SS, Kim SH, Lee KD (2007) Opt Express 15:15457–15463
36. Gordon R, Sinton D, Kavanagh KL, Brolo AG (2008) Acc Chem Res 41:1049–1057
37. Kim TJ, Thio T, Ebbesen TW, Grupp DE, Lezec HJ (1999) Opt Lett 24:256–258
38. Dickson W, Wurtz GA, Evans PR, Pollard RJ, Zayats AV (2008) Nano Lett 8:281–286
39. Liu YJ, Zheng YB, Liou J, Chiang IK, Khoo IC, Huang TJ (2011) J Phys Chem C 115:7717–7722
40. Dintinger J, Robel I, Kamat PV, Genet C, Ebbesen TW (2006) Adv Mater 18:1645–1648
41. Fan YH, Ren H, Liang X, Lin YH, Wu ST (2004) Appl Phys Lett 85:2451–2453
42. Wen CH, Wu ST (2005) Appl Phys Lett 86:231104
43. Graugnard E, Dunham SN, King JS, Lorang D, Jain S, Summers CJ (2007) Appl Phys Lett 91:111101
44. Liu YJ, Hao QZ, Smalley JST, Liou J, Khoo IC, Huang TJ (2010) Appl Phys Lett 97:091101
45. Moharam MG, Grann EB, Pommet DA, Gaylord TK (1995) J Opt Soc Am A 12:1068–1076
46. Johnson PB, Christy RW (1972) Phys Rev B 6:4370–4379

47. Synowicki RA (1998) Thin Solid Film 313–314:394–397
48. Petrossian A, Residori S (2002) Europhys Lett 60:79–85
49. Pishnyak O, Sato S, Lavrentovich OD (2006) Appl Opt 45:4576–4582
50. Mooradian A (1969) Phys Rev Lett 22:185–187
51. Boyd GT, Yu ZH, Shen YR (1986) Phys Rev B 33:7923–7936
52. Xiao M, Rakov N (2003) Phys Lett A 309:452–456
53. Li J, Gauza S, Wu ST (2004) J Appl Phys 96:19–24
54. Huang C-Y, Jhuang W-Y, Hsieh C-T (2008) Opt Express 16:3859–3864
55. Xiang CY, Sun XW, Yin XJ (2003) Appl Phys Lett 83:5154–5156